Supporting Information

Tailoring biomimetic phosphorylcholine-containing block copolymers as membrane-targeting cellular rescue agents

Jia-Yu Wang[1], Wei Chen[2, 3], Michihiro Nagao[4,5], Phullara Shelat[6], Brenton A. G. Hammer[7], Gregory T. Tietjen[8], Kathleen D. Cao[1], J. Michael Henderson[1], Lilin He[9], Binhua Lin[10], Bulent Akgun[4,11,12], Mati Meron[10], Shuo Qian[9], Sarah Ward,[7] Jeremy D. Marks[6], Todd Emrick[7*], Ka Yee C. Lee[1*]*

Affiliations:

[1]Department of Chemistry, Institute for Biophysical Dynamics, James Franck Institute, The University of Chicago, Chicago, Illinois 60637, United States.

[2]Center for Molecular Engineering and Materials Science Division, Argonne National Laboratory, Lemont, Illinois 60439, United States.

[3]Pritzker School of Molecular Engineering, The University of Chicago, Chicago, Illinois 60637, United States.

[4]NIST Center for Neutron Research, National Institute of Standards and Technology, Gaithersburg, Maryland 20899, United States.

[5]Center for Exploration of Energy and Matter, Indiana University, Bloomington, Indiana 47408, United States.

[6]Department of Pediatrics, The University of Chicago, Chicago, Illinois 60637, United States.

[7]Department of Polymer Science and Engineering, University of Massachusetts, Amherst, Massachusetts 01003, United States.

[8]Program in the Biophysical Sciences, Institute for Biophysical Dynamics, The University of Chicago, Chicago, Illinois 60637, United States.

[9]Biology and Soft Matter Division, Oak Ridge National Laboratory, Oak Ridge, Tennessee 37831, United States.

[10]CARS, The University of Chicago, Chicago, Illinois 60637, United States.

[11]Department of Materials Science and Engineering, University of Maryland, College Park, Maryland 20742, United States.

[12]Department of Chemistry, Bogazici University, Bebek, Istanbul 34342, Turkey.

Materials and Methods

Chemicals

Triethylamine (TEA), trimethylamine, 2-bromoisobutyryl bromide, poly(propylene oxide) (M_n = 2,000 g/mol, M_w/M_n = 1.05), 2-[2-(2-chloroethoxy) ethoxy] ethanol, 2,2'-bipyridine, anhydrous methanol, and anhydrous acetonitrile were purchased from Sigma-Aldrich (St. Louis, MO) and used as received. Copper (I) bromide (CuBr) was purchased from Sigma-Aldrich and was sequentially washed with glacial acetic acid, ethanol, and ether (Sigma-Aldrich) before being dried and stored in a desiccator. 2-Hydroxyethyl methacrylate was purchased from Sigma-Aldrich and distilled prior to use. Tetrahydrofuran (THF) was purchased from VWR (Radnor, PA), dried over sodium/benzophenone (Sigma-Aldrich), and freshly distilled before use. 1,2-Dimyristoyl-sn-glycero-3-phosphocholine (DMPC), 1,2-dipalmitoyl-sn-glycero-3-phosphocholine

(DPPC), and 1-palmitoyl-2-oleoyl-sn-glycero-3-phosphocholine (POPC) were purchased in powder from Avanti Polar Lipids (Alabaster, AL) and used as received. DMPC and DPPC spreading solutions were prepared by dissolving lipid powder in chloroform (high-performance liquid chromatography grade, Fisher Scientific, Pittsburgh, PA) at a final concentration of 1 mg/mL and stored at -20 ^{o}C in glass vials. Ultrapure water (resistivity $\geq$ 18 MΩ·cm) was obtained using a Milli-Q UV plus system (A-10 gradient; Millipore, Bedford, MA).

Synthesis of 2-methacryloyloxyethyl phosphorylcholine (MPC)

MPC was synthesized similarly to the procedure as reported by Chen et al.(*1*) ^{1}H NMR (300 MHz, MeOD, δ, ppm): 2.0 (s, 3H), 3.2 (s, 9H), 3.6 (t, 2H), 4.0 (t, 2H), 4.1 (t, 2H), 4.3 (t, 2H), 5.4 (s, 1H), 5.8 (s, 1H) ppm; 31P NMR (300 MHz, MeOD, δ, ppm): 0.0 ppm.

Procedure for the preparation of polyMPC

Ethyl α-bromoisobutyrate (2.50×10^{-2} mL, 1.71×10^{-4} mol) (Sigma-Aldrich), CuBr (5.00×10^{-2} g, 3.42×10^{-4} mol), 2,2'-bipyridine (0.107 g, 6.84×10^{-4} mol), and MPC (1.77 g, 5.95×10^{-3} mol) (the ratio for homopolymer HP_9K[30], where the number in the square bracket represents the number of MPC repeat units per polymer chain) were dissolved in anhydrous methanol (10 mL) in a 25 mL round bottom flask (RBF) packed in ice. Nitrogen was bubbled through the solution for 15 min, then the flask was sealed under a nitrogen atmosphere and the polymerization was run at room temperature for 2.5 h. The polymer was precipitated in anhydrous THF and then purified by silica gel column chromatography with methanol as the eluent. The product was dried under reduced pressure to yield the polymer as white powder with M_n = 9,000 g/mol and M_w/M_n = 1.25 (1.45 g, 82 % yield). ^{1}H NMR (300 MHz, MeOD, δ, ppm): 0.9 to 1.0 (b, 3H), 1.1 to 1.2 (s, 3H), 2.1 (b, 2H), 3.2 (b, 9H), 3.6 (t, 2H), 3.7 (b, 2H), 4.1 (b, 2H,) 4.2 to 4.4 (b, 4H) ppm; ^{31}P NMR (300 MHz, MeOD, δ, ppm): 0.0. Ethyl α-bromoisobutyrate (2.50×10^{-2} mL, 1.71×10^{-4} mol)/MPC (2.43 g, 8.16×10^{-3} mol) yielded HP_13K[43] (M_n = 13,000 g/mol and M_w/M_n =1.30). Ethyl α-

bromoisobutyrate (1.25×10^{-2} mL, 9.00×10^{-5} mol)/ MPC (2.55 g, 8.55×10^{-3} mol) yielded HP_27K[90] (Mn = 27,000 g/mol and M_w/M_n = 1.30).

Preparation of the PPO macro-initiator

PPO (15.0 g, 7.50×10^{-3} mol), TEA (4.20 mL, 3.0×10^{-2}mol), and freshly distilled THF (100 mL) were added to a dried 250 mL 2-neck round bottom flask equipped with a nitrogen inlet and addition funnel. The flask was placed in an ice bath and the solution was stirred for 15 min. 2-Bromoisobutyryl bromide (2.24 mL, 1.80×10^{-2} mol) was added dropwise to the solution over 20 min. The flask was removed from the ice bath and run for 12 h at room temperature. The mixture was passed through a plug of Celite 545 and the solvent was removed by rotary evaporation. The recovered material was purified by silica gel column chromatography with hexane/ethyl acetate (volume ratio of 7/3) as the eluent, and dried under reduced pressure to yield the product as clear oil (14.3 g, 83 % yield). ^{1}H NMR (300 MHz, $CDCl_3$, δ, ppm): 1.1 (b, 3H), 2.0 (s, 12H), 3.3 to 3.5 (b, 3H) ppm. HRMS-FAB (m/z, maximum intensity signal): theoretical = 2298.94g/mol, found = 2300.11 g/mol.

Example procedure for the preparation of polyMPC-PPO-polyMPC

The PPO macro-initiator (0.50 g, 2.20×10^{-4} mol), CuBr (6.31×10^{-2} g, 4.40×10^{-4} mol), 2,2'-bipyridine (0.137 g, 8.80×10^{-4} mol), and MPC (0.95 g, 3.20×10^{-3} mol) were dissolved in anhydrous methanol (5 mL) in a 10 mL round bottom flask cooled in an ice bath. Nitrogen gas was bubbled through the solution for 15 min, then the flask was sealed under a nitrogen atmosphere and the polymerization was run at room temperature for 2.5 h. The polymer was precipitated in anhydrous THF, and purified by silica gel column chromatography eluting with methanol. The product was dried under reduced pressure to yield the polymer BCP_6.5K[14] (the number in the square bracket represents the total number of MPC repeat units per copolymer chain) with M_n = 6,500 g/mol and M_w/M_n =

1.30 as a white powder (1.15 g, 79 % yield). ^{1}H NMR (300 MHz, MeOD, δ, ppm): 0.9 to 1.0 (b, 3H), 1.1 to 1.2 (b, 3H), 1.9 (s, 3H), 2.1 (b, 2H), 3.2 (b, 9H), 3.4 to 3.6 (b, 3H), 3.7 (b, 2H), 4.1 (b, 2H,) 4.2 to 4.4 (b, 4H) ppm. ^{31}P NMR (300 MHz, MeOD, δ, ppm): 0.0 ppm. The PPO macro-initiator (0.25 g, 1.10×10^{-4} mol)/MPC (1.00 g, 3.36×10^{-3} mol) yielded BCP_10.5K[28] (M_n = 10,500 g/mol and M_w/M_n = 1.30); the PPO macro-initiator (0.25 g, 1.10×10^{-4} mol)/MPC (1.55 g, 5.20×10^{-3} mol) yielded BCP_15K[42] (M_n = 15,000 g/mol and M_w/M_n = 1.25); the PPO macro-initiator (0.25 g, 1.10×10^{-4} mol)/MPC (2.25 g, 7.55×10^{-3} mol) yielded BCP_22K[66] (M_n = 22,000 g/mol and M_w/M_n = 1.30); and PPO macro-initiator (0.25 g, 1.10×10^{-4} mol)/MPC (3.00 g, 1.00×10^{-2} mol) yielded BCP_29K[90] (M_n = 29,300 g/mol and M_w/M_n = 1.45).

Preparation of polymer solution

Stock polymer solutions were prepared by adding polymers to ultrapure water, with storage at room temperature overnight to ensure complete dissolution.

Preparation of lipid monolayers

In a typical surface pressure-area isotherm measurement, the lipid monolayer was spread on a Langmuir trough by dropwise addition of the spreading solution at the air/water interface, and then left for 15 min to allow the solvent, chloroform, to evaporate. Following that, the barrier was slowly compressed at a linear speed of 0.1 mm/s until the system reached its target surface pressure. The surface pressure was measured by a Wilhelmy plate-type transducer with a filter-paper plate (R&K, Potsdam, Germany). Assuming that the subphase completely wets the Wilhelmy plate and the thickness (t) of the plate is negligible compared to its width (w), the surface pressure was determined from the force experienced by plate divided by the 2w.

Preparation of large unilamellar vesicles (LUVs)

Large unilamellar vesicles (LUVs) made of DMPC for small angle neutron scattering (SANS) measurements were prepared via the freeze-thaw extrusion method. Initially, phospholipids in chloroform were dried under ultrapure argon to redisperse lipids as a thin film coating the interior of the glass vial. After being kept under vacuum for at least 1 h, the dry lipids were rehydrated in ultrapure water to a desired concentration and then mixed vigorously by vortexing at room temperature for 1 h to emulsify the lipid. Following that, the LUV solution was completely frozen in a dry-ice/ethanol bath for ≈ 1 min and then gently thawed in warm water (> 50 °C) for ≈ 30 s. This freeze-thaw process was repeated at least five times. Then the solution was extruded at least 41 times through a polycarbonate filter with the average pore size of 100 nm in diameter to form LUVs. The typical diameter of the LUVs, determined by dynamic light scattering (DLS), was centered at (130±30) nm. Liposomes were then stored at 37 °C in an oven and in general good for use within a week of their formation.

Preparation of dye-loaded giant unilamellar vesicles (GUVs)

20 μL of the POPC solution with a concentration of 2.5 mg/mL was spread on glass slides coated with indium tin oxide (Resistance = 70Ω to 100 Ω, Delta Technologies, Limited). The solvent was then evaporated for 30 min under vacuum. Two slides separated by a Teflon spacer of 0.5 mm were assembled to form the sealed electroformation chamber. The chamber was filled with the aqueous solution which contained, in general, 3 % Alexa Fluor® 488 hydrazide and 300 mmol/L sucrose. An AC voltage of 10 Hz was applied immediately to the ITO slides and the voltage was progressively increased from 0.2 V to 1.2 V within 40 min and then kept constant at 1.2 V for 30 min. The frequency was finally decreased to 4 Hz with the voltage of 1.0 V for 0.5 h to 1 h to detach GUVs from the glass slides. The vesicles were then diluted in a medium containing 300 mmol/L glucose. The difference in density between sucrose and glucose facilitated GUVs sedimentation, allowing them to be easily separated from their dispersion medium. In general, 3 to 5 times of centrifugal separation were applied to the GUVs to remove Alexa 488 in the dispersion medium. The vesicles, either in sucrose or glucose solution, were usually good for use within a week of their formation.

Postnatal hippocampal neuronal cultures

Hippocampal neurons were prepared and maintained as previously described (*2*). Briefly, under isoflurane-induced anesthesia, day 17 embryos were extracted from timed-pregnant Sprague–Dawley rats. The hippocampi were then removed, sectioned and incubated in oxygenated, pH-buffered saline. After trypsin digestion, the hippocampi were mechanically dissociated, centrifuged, and then plated onto poly-L-lysine-coated coverslips with a neuronal density of $\approx 4\times10^4$ cells/mL. Following that, the coverslips were placed into Petri dishes containing the neurobasal medium with 2 % B-27 supplement, 0.5 mmol/l-glutamine, and 0.025 mmol/l L-glutamate and incubated in a conventional humidified 5 % CO_2 incubator at 37 ^oC. To inhibit glial proliferation, cytosine-β-D-arabinofuranoside was added to the culture medium after 72 h of incubation. All neurons used in this work were between 12 days and 14 days of division.

Oxygen glucose deprivation (OGD) model

OGD experiments were performed in the culture medium that was replaced by thorough exchange with deoxygenated glucose-free bicarbonate-buffered saline containing 95 mmol/L NaCl, 5.3 mmol/L KCl, 1.3 mmol/L NaH_2PO_4, 1.3 mmol/L $MgSO_4$, 24 mmol/L $NaHCO_3$, and 2.4 mmol/L $CaCl_2$. To prepare saline for OGD experiments, the bicarbonate buffer was incubated in a hypoxia workstation (Coy Laboratory Products, Grass Lake MI), where O_2 and CO_2 levels were continuously maintained at 1 % and 5 %, respectively. For control experiments without OGD challenge, the bicarbonate buffer with 25 mmol/L glucose and 1 mmol/L succinate was incubated in the conventional humidified 5 % CO_2 incubator. Both saline solutions were incubated under their environmental conditions for 18 h before transferring cultured neurons to them. The *in vitro* cellular experiments were performed by incubation of neurons either under the OGD condition or in the control saline solution for 45 min. After that, the neurons were transferred back to their original neurobasal medium where polyMPC homopolymer or polyMPC-PPO-polyMPC was introduced to study the potential of these polymers in rescuing injured

neurons from hypoxic injury. Before each experiment, dead neurons were removed by incubation of neurons in DNase (15 μkatal/ml) for 1 h.

Evaluation of neuronal survival

Cell survival was evaluated using unbiased automated total-live cell assay 48 h after transferring neurons back to their original neurobasal medium. Briefly, cells stained by 4',6-diamidino-2-phenylindole (DAPI) and calcein acetoxymethylester (calcein-AM) were observed under epifluorescence at wavelengths of 450 nm and 536 nm with a 20× Fluor objective in an inverted microscope (Nikon, Tokyo, Japan) and imaged with a cooled CCD camera (Photometrics, Tucson, AZ) connected to a computer workstation running the high-content screening system, ImageXpress micro (Molecular Devices, PA). DAPI stains nuclei of both live and dead cells; calcein-AM, a cell-permeable dye, stains the body of live cells via converting the initially nonfluorescent dye to a green-fluorescent calcein by intracellular esterases that are only present in live cells. Therefore, neurons stained by both DAPI (blue) and calcein (green) are identified as live, whereas neurons stained only by DAPI (blue) are categorized as dead. To estimate neuron survival, live and dead cells were counted in fluorescence micrographs using MetaXpress cellular analysis software (Molecular Devices, Downingtown, PA). In general, at least 42 equally distributed fields that contain at least 1300 neurons from at least six coverslips for each condition in each experiment were counted. To make DAPI distinguishable from calcein, false coloring with magenta, instead of its native color, blue, was used in the micrographs. The statistical analysis was performed by one-way analysis of variance (ANOVA) followed by the Tukey test. $p < 0.05$ were accepted as significant.

Equilibrium spreading pressure measurements

The polymer surface activity and critical micelle concentration (CMC) were evaluated by examining its equilibrium spreading pressure (ESP) at the air/water interface as a function of polymer concentration. In general, multiple injection experiments were performed separately, each with injection of a gradually increasing amount of polymers

into the water subphase. Each time after polymer injection, the system was left undisturbed until it reached its equilibrium and the corresponding surface pressure was recorded as the ESP at that concentration. Because no significant increases in ESP above a certain polymer concentration signifies the equilibrium between polymer unimers and micelles in the subphase, this particular polymer concentration in the subphase is recorded as the CMC and the corresponding surface pressure is recorded as the maximum surface pressure, π_{max}, that this polymer can reach.

Evaluation of polymer surface activity and critical micelle concentration

The surface activity of polyMPC homopolymer and polyMPC-PPO-polyMPC was monitored through their adsorption kinetics at the air-water interface. In general, adsorption experiments at a constant surface area were performed in a home-made Teflon trough with a subphase volume of 50 mL. A given volume of an aqueous polymer solution enough for reaching the desired end polymer concentration was injected into the subphase with a Hamilton syringe and L-shape needle through the gap between the barrier and the bottom of the trough. To accelerate the homogeneous distribution of the polymer throughout the subphase without perturbing the surface, the L-shape needle was used to gently stir the subphase right after polymer injection. The change in surface pressure, π, due to polymer adsorption was measured using a Langmuir surface balance with a precision of 0.01 mN/m. The reproducibility of adsorption experiments was estimated to be 0.5 mN/m. The temperature of the trough was maintained constant at (25$\pm$1) ^{o}C.

The critical micelle concentration (CMC) was evaluated by examining its equilibrium spreading pressure (ESP) at the air/water interface as a function of polymer concentration. In general, multiple injection experiments were performed separately, each with injection of a gradually increasing the amount of polymers into the water subphase. Each time after polymer injection, the system was left undisturbed until it reached its equilibrium and the corresponding surface pressure was recorded as the ESP at that concentration. Because no significant increases in ESP above a certain polymer concentration signifies the equilibrium between polymer unimers and micelles in the

subphase, this particular polymer concentration in the subphase is recorded as the CMC and the corresponding surface pressure is recorded as the maximum surface pressure, π_{max}, that this polymer can reach.

Constant surface pressure insertion assay

The quantification of polymer insertion into lipid monolayers was done through a constant pressure insertion assay. In general, lipid monolayers were prepared and kept at π = 30 mN/m, a bilayer equivalent pressure, *via* a built-in feedback system that adjusts the surface area. The polyMPC homopolymers or polyMPC-PPO-polyMPC block copolymers were injected into the subphase, similar to the procedure for the evaluation of polymer surface activity. If the injected polymer interacts with lipids through membrane insertion, π would increase. To keep π constant, A has to increase. Thus, the relative area change, $\Delta A/A_0$, reflects the degree of polymer insertion into the lipid film.

Both polymer Gibbs adsorption isotherms and lipid surface pressure-area isotherms were measured using a Langmuir surface balance (Rieger & Kirstein, Berlin, Germany), which consists of a home-built Teflon trough with one movable barrier and one Wilhelmy plate made of filter paper. The barrier serves for the control of the area of interest and the Wilhelmy plate measures the change in surface pressure, π, accompanied by the change in surface area. Here, π is defined as γ_s-γ_m, where γ_s and γ_m are surface tensions of a pure clean subphase and one with a monolayer adsorbed, respectively. For this work, the surface tension of the subphase, γ_s, is that of pure water, which is 72 mN/m at 25 ^{o}C. The temperature was controlled by a series of thermoelectric units (Omega Engineering Inc., Stamford CT) and a water circulator held at 20 °C (Neslab RTE-100; Portsmouth, NH). The entire set-up is controlled by a custom software interface designed using Lab View 6.0 (National Instruments, Dallas, TX).

Atomic force microscopy (AFM) imaging

To image monolayers of DPPC, DPPC+BCP_22K[66], and DPPC+BCP_6.5K[14] with AFM, lipid monolayers at 30 mN/m and 25 ^{o}C were transferred from the air/water interface to high-quality mica substrates by an inverted Langmuir-Schaeffer method. This procedure yields a supported monolayer with polar headgroups in contact with the mica surface and hydrophobic tails exposed to the air. After deposition, the supported monolayers were dried at 25 ^{o}C before measurements.

DPPC monolayers transferred to mica substrates were imaged at room temperature using a Multimode Nanoscope IIIA scanning probe microscope (Digital Instruments, Santa Barbara, CA) with a Type J scanner in contact mode in air. Silicon nitride tips NP-S (Veeco Probes, Woodbury, NY) with a nominal spring constant of 0.32 N/m were used; the surface of the tips was decontaminated by ultraviolet-generated ozone before sampling (PSD-UV Surface Decontamination System, Novascan, Ames, IA).

Leakage assay

The dye-loaded GUVs prepared above were exposed to glucose-plus-polymer solutions with the final polymer concentration of 30 μmol/L. As only a trace of Alexa 488 is left in the dispersion medium after the centrifugal separation, leakage can be monitored via the fluorescence increase in the dispersion medium of GUVs. In our case, leakage was qualitatively defined by $I/I_0 > 1$, where I_0 is the fluorescence intensity of the dispersion medium of GUVs without polymers. For all the measurements, vesicle concentrations were kept identical and leakage measurements for each sample were averaged over at least ten runs using two separate batches of vesicles.

To monitor fluorescence intensity in the leakage assay, a vertical optical microscope (Nikon ME600) with a cooled CCD camera (Hamamatsu ORCA-ER) connected to a PC running the Simple PCI software (Compix Inc. Sewichley, PA) was used. For these measurements, only fluorescence intensity in regions of interest (*3*) (*3*),

that is, regions without GUVs were integrated. Typically, 20 different ROIs were recorded for each sample.

Instrumentation

Polymer characterization

^{1}H NMR spectra were recorded on a Brüker-SpectroSpin 300 using the residual proton resonance of the solvent as the internal standard. Polymer molecular weight was estimated by gel permeation chromatography (GPC) using 0.1 mol/l $NaNO_3$ and a weight fraction of 10 % $NaNO_3$ in water as the eluent against poly(ethylene oxide) (PEO) standards with a refractive index detector.

Neutron spin echo (NSE)

NSE measurements were performed using the NG5-NSE spectrometer (*4, 5*) at the Center for Neutron Research (NCNR) of National Institute of Standards and Technology (NIST, USA). The 8 Å incident neutron beam was mechanically selected with wavelength resolution of approximately 20 %. A set of polarizers and analyzers were used in order to analyze the neutron polarization. The Larmor precession of neutron spin in a magnetic field was used as a precise measure of energy transfer between the neutrons and the sample. The covered ranges of momentum transfer, q, and time, t, were 0.04 $Å^{-1} < q < 0.13$ $Å^{-1}$ and 0.5 ns ≤ t ≤ 40 ns, respectively. The sample thickness was 2 mm, loaded in NCNR-standard titanium cells with quartz windows. The NSE measurements were taken at 37 °C, 25 °C, 23 °C and 15 °C; each temperature was controlled with the accuracy of ± 0.1 °C. The DAVE software package (NCNR, NIST) was used for data reduction to correct background and experimental resolution and to convert the echo signal to the normalized intermediate scattering function, $I(q, t)/I(q, 0)$ (*6*).

To analyze the NSE data, the ZG model (*7*) and Zimm model (*8*) were used. NES directly measures the intermediate scattering function $I(q,t)$ that originates from

fluctuations of lipid membranes and the Zimm dynamics of polymer chains. The normalized intermediate dynamic structure factor of a membrane at a q region that is sensitive to single membrane dynamics can be predicted by the theory proposed by Zilman and Granek (ZG model) (*7*) and expressed as

$$\left[\frac{I(q,t)}{I(q,0)}\right]_{ZG} = \exp\left[-(\Gamma(q)_{ZG}t)^{2/3}\right], \quad (1)$$

and the effective bending modulus, $\tilde{\kappa}$, can be obtained from the decay rate $\Gamma(q)_{ZG}$, which follows the q^3 dependence as

$$\Gamma(q)_{ZG} = 0.025\gamma\left(\frac{k_BT}{\tilde{\kappa}}\right)^{1/2}\frac{k_BT}{\eta}q^3. \quad (2)$$

Here, γ is a function of k_BT and approaches unity for $\tilde{\kappa}/k_BT \gg 1$, k_B is the Boltzmann constant, T is the temperature, and η is the solvent viscosity. The effective bending modulus $\tilde{\kappa}$ includes the interlayer friction contribution to the membrane stiffness, which appears as $\tilde{\kappa} = \kappa + 2d^2k_m$, where κ, d, and k_m are the intrinsic bending modulus, the height of the neutral surface from the bilayer midplane, and the monolayer lateral compressibility modulus, respectively (*9*). Following the treatment by Woodka et al. (*10*), we used the relations, $d = 0.65d_{tail}$ and $k_m = 24\kappa/(d_{tail})^2$, where d_{tail} is the length of the tail region of DMPC membranes and its value was obtained from small angle neutron scattering (SANS) measurements (Fig. S4-I). It should be noted that the addition of 200 μmol/LHP_27K[90] did not change the value of d and viscosity of D_2O, η_{D2O} (η_{D2O} = 1.210 mPa·s; $\eta_{D2O+HP\_27K[90]}$ = 1.211 mPa·s at 24 °C).

The dynamics of polymer chains in dilute solution can be described by the Zimm model (*8*) which contains the hydrodynamic coupling of chain segments and entropic forces between them as main ingredients. The normalized intermediate scattering function of the Zimm model was theoretically calculated by de Gennes and Dubois-Violette (*11*) and is given by

$$\left[\frac{I(q,t)}{I(q,0)}\right]_{\text{Zimm}} = \int_0^\infty du \exp\left\{-u - (\Gamma(q)_{\text{zimm}}t)^{2/3} h\left[\frac{u}{\Gamma(q)_{\text{Zimm}}t}\right]\right\} \quad (3)$$

where $h(y) = \frac{4}{\pi}\int_0^\infty dx \frac{cosx^2}{x^3}\left[1 - \exp\left(-y^{-3/2}x^3\right)\right]$, and $\Gamma(q)_{\text{Zimm}} = \frac{1}{6\pi}\frac{k_B T}{\eta} q^3$.

Because the total intermediate scattering of lipid membranes in the presence of HP_27K[90] were contributed from both lipid membranes and polymer chains, its overall normalized intermediate scattering function can be expressed as $\frac{I(q,t)}{I(q,0)} = (1-f)\left[\frac{I(q,t)}{I(q,0)}\right]_{\text{ZG}} + f\left[\frac{I(q,t)}{I(q,0)}\right]_{\text{Zimm}}$, where *f* is the fraction of the contribution from polymer chains dynamics in solution and was estimated from SANS intensity at the corresponding *q* values.

Small-angle neutron scattering (SANS)

SANS experiments were conducted on the NG7-SANS instrument at NCNR-NIST (NIST, USA) (*12, 13*) and the CG-3 Bio-SANS instrument of the High Flux Isotope Reactor (HFIR) at Oak Ridge National Laboratory (ORNL) (*14*). The incident neutron wavelength, λ, at NIST was selected to be 6 Å for 1 m and 4 m configurations and 8.9 Å for 15.3 m configuration, with a wavelength resolution of approximately 11 %. λ at ORNL was selected to be 6 Å for 1.1 m and 6.8 m configurations and 12 Å for 15.3 m configuration, with a wavelength resolution of approximately 15 %. With these configurations, *q* was measured from 0.001 $Å^{-1}$ to 0.557 $Å^{-1}$ at NIST and 0.002 $Å^{-1}$ to 0.717 $Å^{-1}$ at ORNL. The sample thickness was 1 mm, loaded in standard quartz banjo cells (Hellma USA, Plainview, NY) and mounted in a temperature-controlled cell holder with accuracy of 0.1 °C at NIST and 1 °C at ORNL. The observed two-dimensional data were corrected for background scattering, azimuthally averaged, and normalized to an absolute intensity using the SANS data reduction program developed at NIST (*15*) and ORNL. For all SANS data, background scattering from D_2O was subtracted, and the one-dimensional scattering intensity *I(q)* was obtained by radial averaging of the corrected 2-D data. All SANS data analysis was performed using SansView (http://danse.chem.utk.edu.).

For SANS analysis, the SANS intensity of DMPC LUVs was approximately estimated as $I(q) = N_p V_p^2 (\Delta\rho)^2 P(q) S(q) + I_{inc}$, where N_p is the number concentration of scattering bodies (the subscript 'P refers to 'particles'), V_p is the volume of one scattering body, $P(q)$ is a function known as the form or shape factor, $S(q)$ is the inter-particle structure factor, I_{inc} is the (isotropic) incoherent background signal, and $(\Delta\rho)^2$ is the square of the difference in neutron scattering length density. In order to take into account of the influence of vesicle size polydispersity, the size distribution function, $f(r)$, is assumed to be the Schulz distribution, $f(r) = \left(\frac{z+1}{r_m}\right)^{z+1} \frac{r^z}{\Gamma(z+1)} \exp\left[\frac{-r(z+1)}{r_m}\right]$, where r_m is the mean radius, z is a parameter related to the width of the distribution. In particular, one has a polydispersity index $\rho = \sigma_r / r_m$, where σ_r is the root-mean-square deviation from the mean size, given by $\rho = 1/(z+1)^{1/2}$. $\Gamma(x)$ represents the gamma function. The polymer contribution to the scattering intensities was subtracted from the measured scattering intensities.

Grazing incidence x-ray diffraction (GIXD) and x-ray reflectivity (XR)

GIXD and XR experiments were performed at the Advanced Photon Source (APS) of Argonne National Laboratory using ChemMatCARS in Sector 15-ID-C. The wavelength of the x-ray beam was 1.24 Å, corresponding to the energy of 10 keV. A Langmuir trough, equipped with a Wilhelmy balance and a barrier for surface pressure control, was mounted on the diffractometer. The trough was enclosed in a sealed canister flushed with helium to achieve an oxygen level below 1 %; this reduced the scattering background and minimized possible oxidative beam damage during x-ray scans. As a further precaution against beam damage, the trough was translated by 2 mm horizontally across the x-ray beam, in the direction along the barrier compression at every step of the scan. All the measurements were done at (23±1) °C. The data reduction was done through IDL software with the customized programs and the data were analyzed using the program of Motofit (*16*).

For GIXD, it measures the scattered intensity that scans over a range of horizontal scattering vector components: $q_{xy} \approx 2\pi/\lambda \sqrt{1+\cos^2\alpha_f - 2\cos\alpha_f \cos 2\theta_{xy}}$, where q_{xy} is the in-plane

scattering vector, λ is the x-ray wavelength, α_f is the vertical scatting angle, and $2\theta_{xy}$ is the angle between the incident and diffracted beams projected on the liquid surface. Bragg peaks, resolved in q_{xy}, are obtained by integrating the scattered intensity over the range of interest that is perpendicular to the interface (i.e., along $q_z = 2\pi/\lambda(\sin\alpha_i + \sin\alpha_f) = 4\pi/\lambda\sin\alpha_f$, where α_i is the incidence angle). Conversely, Bragg rod profiles are extracted, after background subtraction, by integrating the scattered intensity across a Bragg peak. The angular positions of Bragg peaks determine d-spacings $d_{hk} = 2\pi/q_{xy}$ for a 2D lattice. The full width at half maximum (FWHM) of Bragg peaks determine the 2D crystalline coherence length, L_{xy}, that is, the average distance over which crystallinity extends. Here, $L_{xy}=0.9\times2\pi/(\mathrm{FWHM}q_{xy}^2-\mathrm{FWHM}_{resol}^2)^{1/2}$, where FWHM_{resol} is the instrumental resolution. The intensity distribution along the Bragg rod determines the direction and magnitude of the molecular tilt as well as the out-of-plane coherence length $L_c = 0.9\times2\pi/(\mathrm{FWHM}q_z^2-\mathrm{FWHM}_{resol}^2)^{1/2}$, that is, the length of molecules that scatter coherently. Here q_z is the vertical scattering vector.

For XR, it yields detailed information on the electron density distribution normal to the interface, $\rho_e(z)$, laterally averaged over both the ordered and disordered parts of the film. In our analysis, a slab model is used in which the monolayer is represented as a stack of slabs, each slab having a constant $\rho_e(z)$ and thickness, t. The interfaces between slabs are smeared out by convolution with the standard deviation of the error function, σ, that accounts for roughness at the boundary due to thermally excited capillary waves as well as additional local interfacial diffuseness.

Neutron reflectivity (NR)

NR measurements were performed using the NG7 reflectometer at the NCNR, NIST (NIST, USA). To collect NR data, a fixed wavelength of 4.75 Å was used and the height of the slits was varied to maximize the beam intensity while keeping a constant beam footprint and relative q-resolution ($\delta q/q$ = 0.04) throughout the whole q range. A Langmuir trough (KSV 5000), equipped with a Wilhelmy balance and a barrier for surface pressure control, was mounted on the diffractometer. The trough was enclosed in a

sealed canister to minimize evaporation. All the measurements were made at (25±0.5) ^{o}C. The programs from the reflpak suite were used for data reduction (*17*) and the data were analyzed using the program of Motofit (*17*).

Just like XR, NR also determines the structure of a film perpendicular to the air-water interface, but it detects the variation in scattering length density (SLD) as a function of depth. Because SLD of hydrogen is very different from its isotope deuterium, the proper use of contrast variation methods allows for the detection of the thickness and composition of specific interfacial layers with high accuracy. Thus, the combined use of XR and NR makes them good complementary techniques for characterizing lipid/polymer systems. Similar to XR, the analysis of NR data uses the slab model described above as well.

Surface Force Apparatus (SFA)

The normal and friction forces between two DPPC bilayers grafted on mica were measured using a surface force apparatus (SFA 2000, SurForce LLC). Normal forces in solution were measured as a function of the distance between the opposing mica substrates in a cross-cylinder geometry.

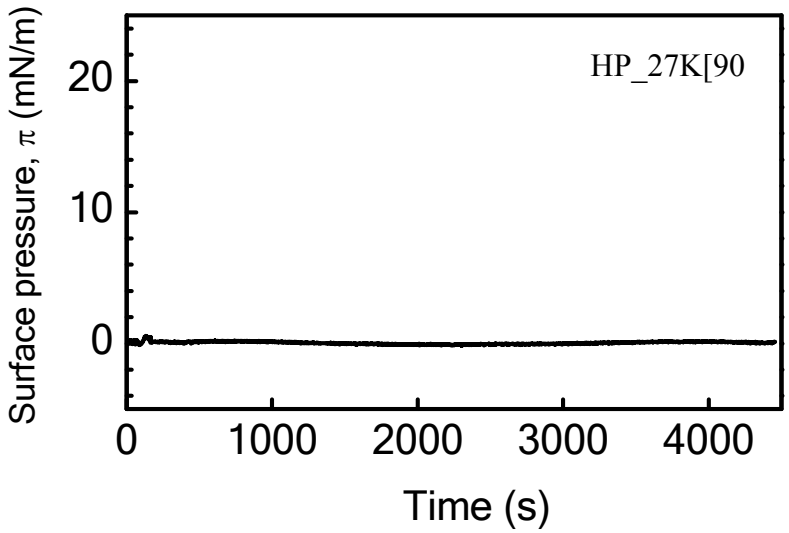

Fig. S1 A representative Gibbs adsorption isotherm of polyMPC homopolymer at the air/water interface and 25 °C. The final polymer concentration in the water subphase is 200 μmol/L. π = 0 indicates no surface activity for polyMPC homopolymers.

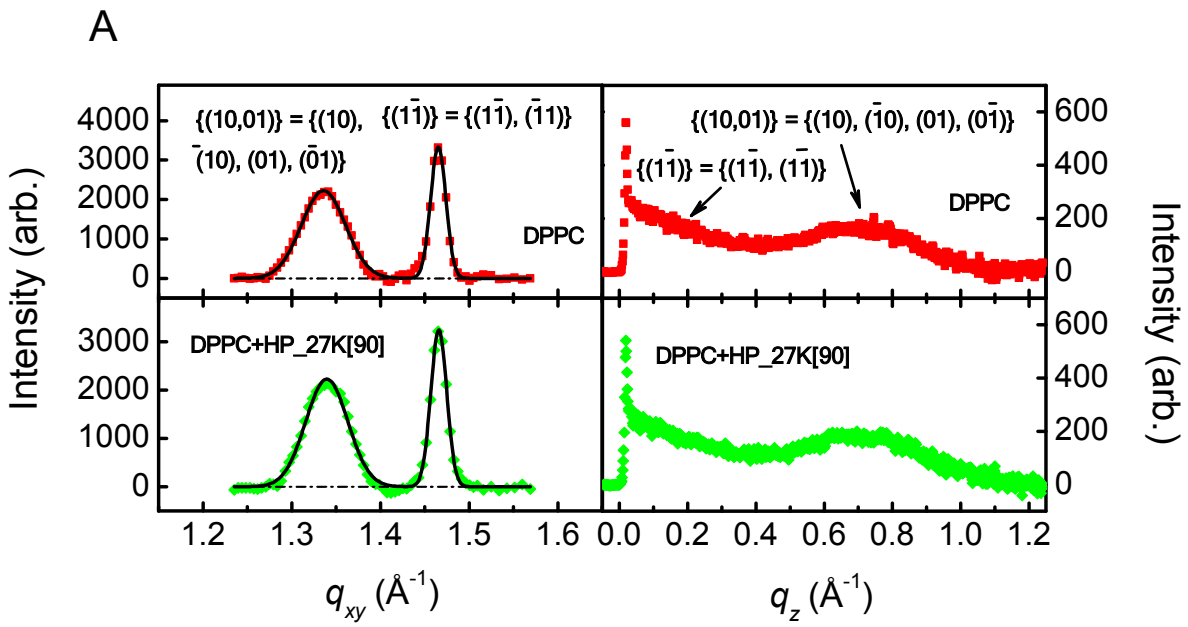

B

composition	in-plane Bragg peaks					out-of-plan Bragg Rods
	a, b (Å)	γ (^{o})	$A_{unit\ cell}$ (Å^{2})	coherence length (Å) L_{10}	L_{11}	tilt angle Θ (^{o})
DPPC	5.13	114	24.1	97	307	30.1
DPPC_HP_27K[90]	5.12	114	24.0	102	318	29.7

Fig. S2 (A) Bragg peaks (left) and rods (right) from GIXD of DPPC and DPPC+HP_27K[90] monolayers on pure water at π = 30 mN/m and T = 23 ºC. (B) Parameters obtained from the GIXD profiles. The GIXD measurements were taken at A_{DPPC} = 46.4 Å^2 and $A_{DPPC+HP\_27K[90]}$ = 46.1 Å^2. The final concentration of HP_27K[90] in the water subphase is 100 μmol/L. The two Bragg peaks from the DPPC monolayer at q_{xy} = 1.34 Å^{-1} (from the {(10, 01)} reflection) and 1.47 Å^{-1} (from the {(1$\bar{1}$)} reflection) indicate that DPPC molecules at this surface pressure primarily pack in a distorted hexagonal unit cell (*18*). Through the relationship of $d = 2\pi/q_{xy}$, where d is the d-spacing and q_{xy} is the in-plane scattering wave vector, the corresponding d-spacings of 4.7 Å and 4.3 Å were obtained for the pure DPPC monolayer, giving a unit cell with axes $a = b$ = 5.13 Å, angle γ = 114^{o} (the angle across from the a and b axis), and the unit cell area $A_{unit\ cell}$ = 24.1 Å^2. From the full wave at half maximum (FWHM) of the Bragg peaks, the coherence lengths, L_{10} and L_{11}, were calculated to be 97 Å and 307 Å in the crystallographic directions of {(10, 01)} and {1$\bar{1}$}, respectively, and the molecular tilt angle, θ, analyzed from the Bragg rod was found to be 30.1^{o}. Upon introducing HP_27K[90] to the water subphase, the GIXD profile of DPPC+HP_27K[90] shows little change in comparison with those of pure DPPC, indicating that the HP_27K[90] polymer barely affects lateral packing of DPPC molecules.

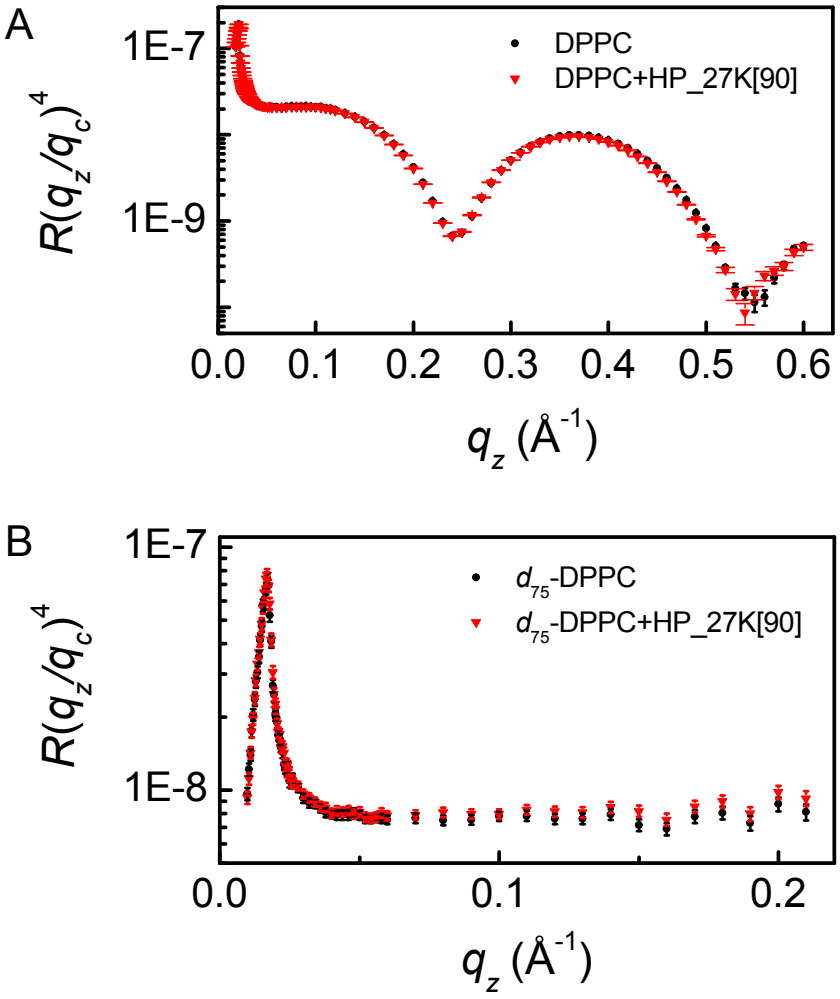

Fig. S3 (A) XR of DPPC and DPPC+HP_27K[90] monolayers on pure water at π = 30 mN/m and T = 22 ºC. (B) NR of d_{75}-DPPC and d_{75}-DPPC+HP_27K[90] on D_2O at π = 30

mN/m and T = 25 ºC. The x axis, q_z, is normalized by the critical q_c calculated from pure water or D_2O; the y axis is the reflected intensity, R, multiplied by $(q_z/q_c)^4$. XR experiments were performed on DPPC on pure water at A_{DPPC} = 46.4 Å^2 and $A_{DPPC+HP\text{-}27K[90]}$ = 46.0 Å^2, and the NR experiments were performed on d_{75}-DPPC on D_2O at $A_{d75\text{-}DPPC}$ = 47.0 Å^2 and $A_{d75\text{-}DPPC+HP\_27K[90]}$ = 46.0 Å^2. The final concentration of HP_27K[90] in the water/D_2O subphase is 100 μmol/L. Because the scattering length density (SLD) of d_{75}-DPPC is comparable to D_2O, the use of this contrast matching strategy provides better resolution than XR in detecting any membrane structural change normal to the air-water interface induced by the hydrogenated HP_27K[90]. However, no detectable difference between DPPC and DPPC+HP_27K[90] were seen in both XR and NR profiles. Thus the combination of GIXD, XR and NR results indicates that this polymer has little influence on lateral packing of DPPC molecules. Error bars represent ±1 standard deviation in the present supplemental material.

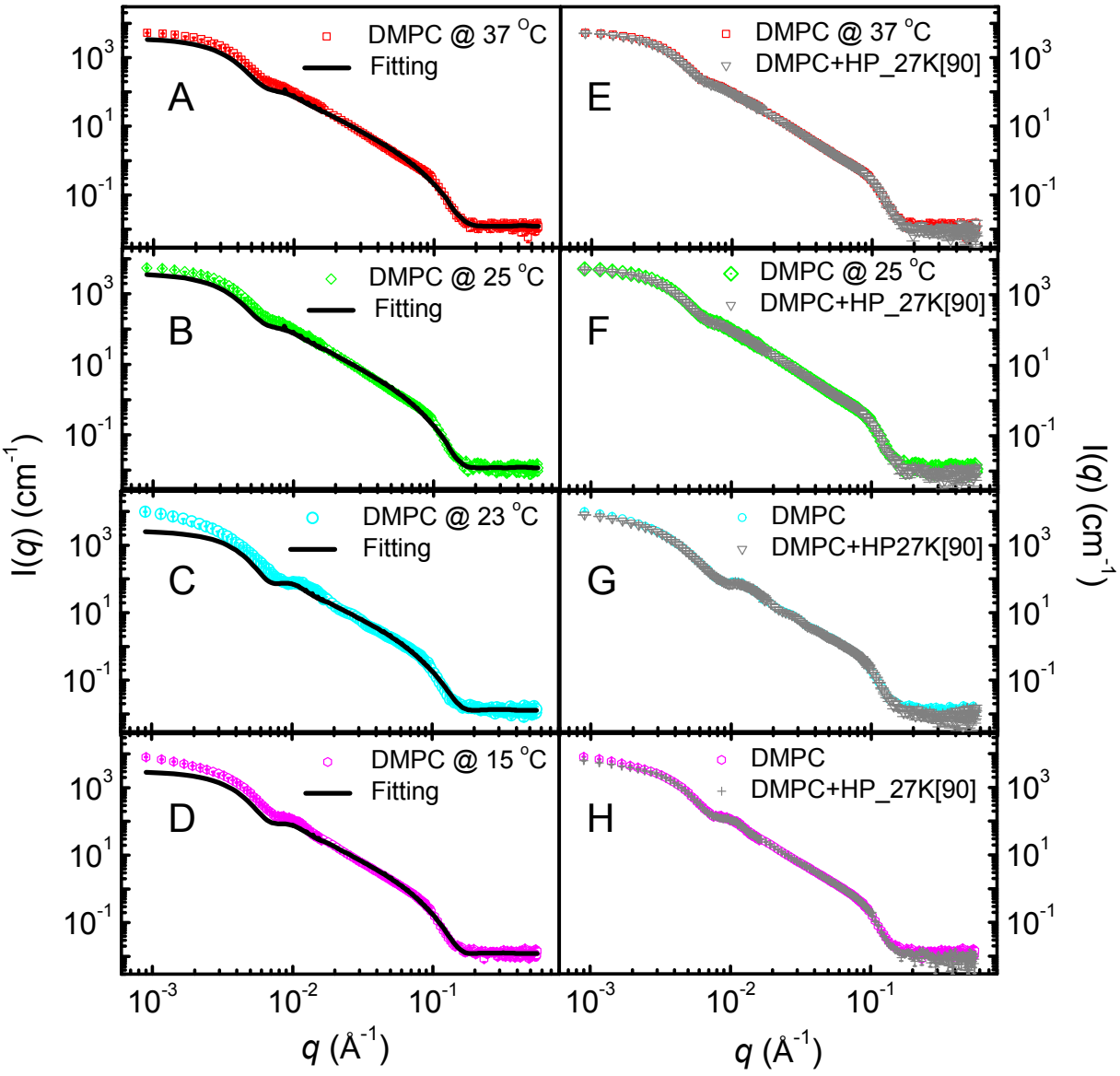

I

sample	T (°C)	d_{full} (Å)	d_{head_I} (Å)	d_{head_O} (Å)	d_{tail} (Å)
DMPC	37	48.7±0.3	13.0±0.1	13.1±0.2	22.6±0.2

25	49.6±0.2	12.9±0.1	13.6±0.1	23.1±0.1
23	55.3±0.3	12.4±0.2	12.8±0.2	30.1±0.1
15	54.6±0.4	11.7±0.3	12.6±0.2	30.3±0.1

Fig. S4 SANS of DMPC LUVs (A-D) and DMPC LUVs in the presence of 200 μmol/L HP_27K[90] (E-H) at 37 ºC (A, E), 25 ºC (B, F), 23 ºC (C, G) and 15 ºC (D, H). For profiles of DMPC in the presence of HP_27K[90], scattering contributed from the polymer was subtracted. The asymmetric three-shell vesicle model was used to fit DMPC profiles (straight line) and the fitting parameters are listed in (I). d_{full}, d_{head_I}, d_{head_O} and d_{tail} indicate thicknesses of the entire bilayer, head of the inner leaflet, head of the outer leaflet and tail regions of the membrane, respectively. The concentration of DMPC is 10 mg/mL. For SANS analysis, we assumed that the DMPC LUVs follow the Schulz distribution of radii with three layers, each with a corresponding scattering length density (SLD). The two outer layers of the membrane represent the hydrogenated lipid headgroup regions and were allowed to have different thickness and SLD; the third (center) layer represents the lipid tail region. The black line in the figures represents the best fits and the fitting parameters for each temperature are summarized in Figure-S4-I. It should be noted that the thickness of the lipid membranes was mainly determined by $q > 0.03$ Å^{-1}; therefore, the slight difference between experimental data and the fitting curve at $q < 0.01$ Å^{-1} does not affect our analysis of membrane thickness. It can be seen that d_{full} and d_{tail} decrease with temperature but d_{head} increases with temperature, indicating that lipids at these temperatures pack very differently, which is consistent with previous studies (*10*). Upon introducing HP_27K[90], the SANS profiles at the four temperatures all show no detectable change in comparison with those of pure LUVs, suggesting the polymer, regardless of lipid packing density and membrane curvature, has little influence, if at all, on membrane static structure, in good agreement with GIXD, XR and NR measurements on lipid monolayers.

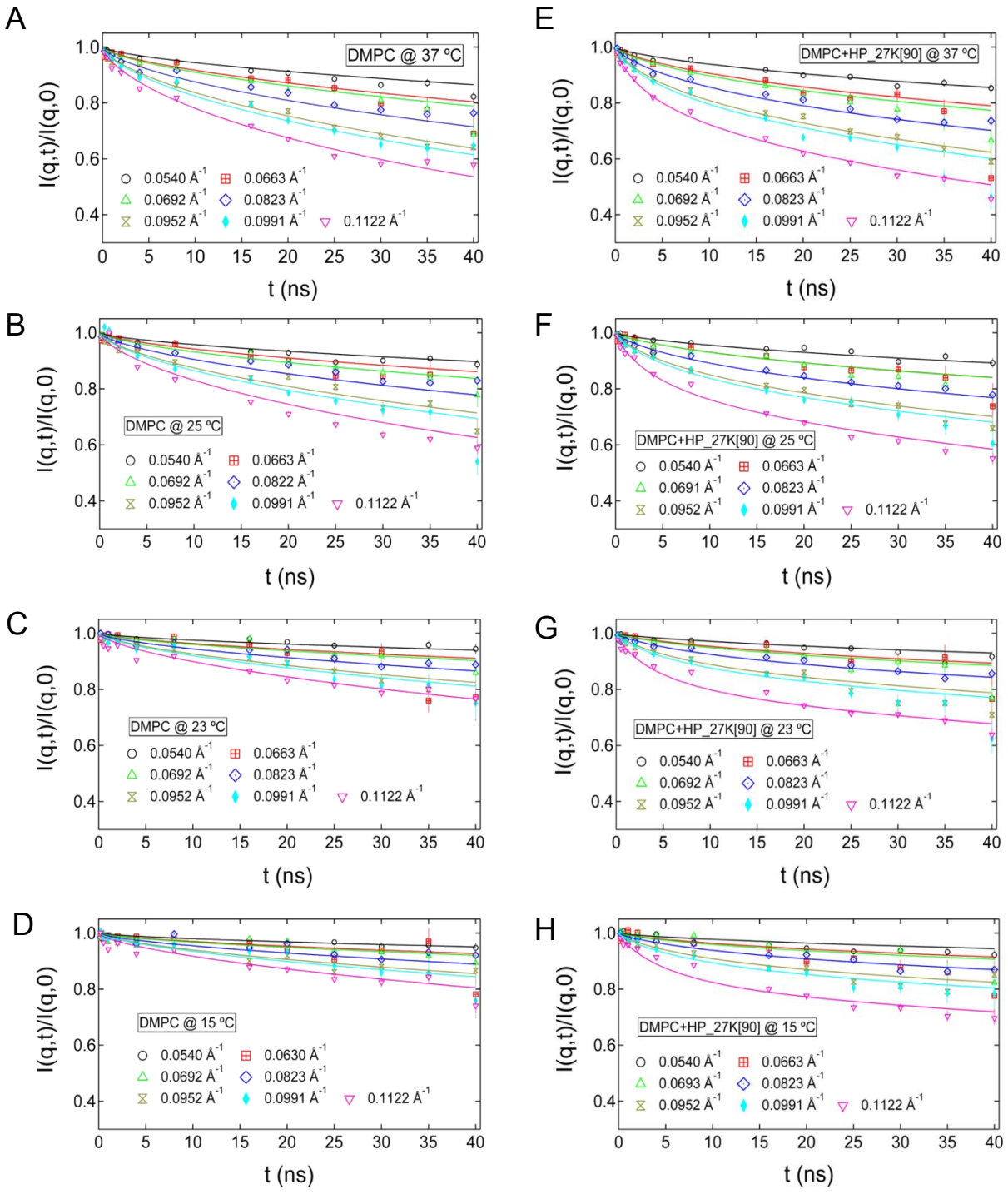

Fig. S5 Normalized intermediate scattering function of DMPC LUVs (A-D) and LUVs in the presence of 200 μmol/L HP_27K[90] (E-H) at 37 ºC (A, E), 25 ºC (B, F), 23 ºC (C, G), and 15 ºC (D, H). Fits are to the Zilman and Granek model for (A-D) and to the linear combination of membrane undulation and polymer dynamics for (E-H). The concentration

of DMPC is 20 mg/mL; error bars represent ±1 standard deviation in the present supplemental material.

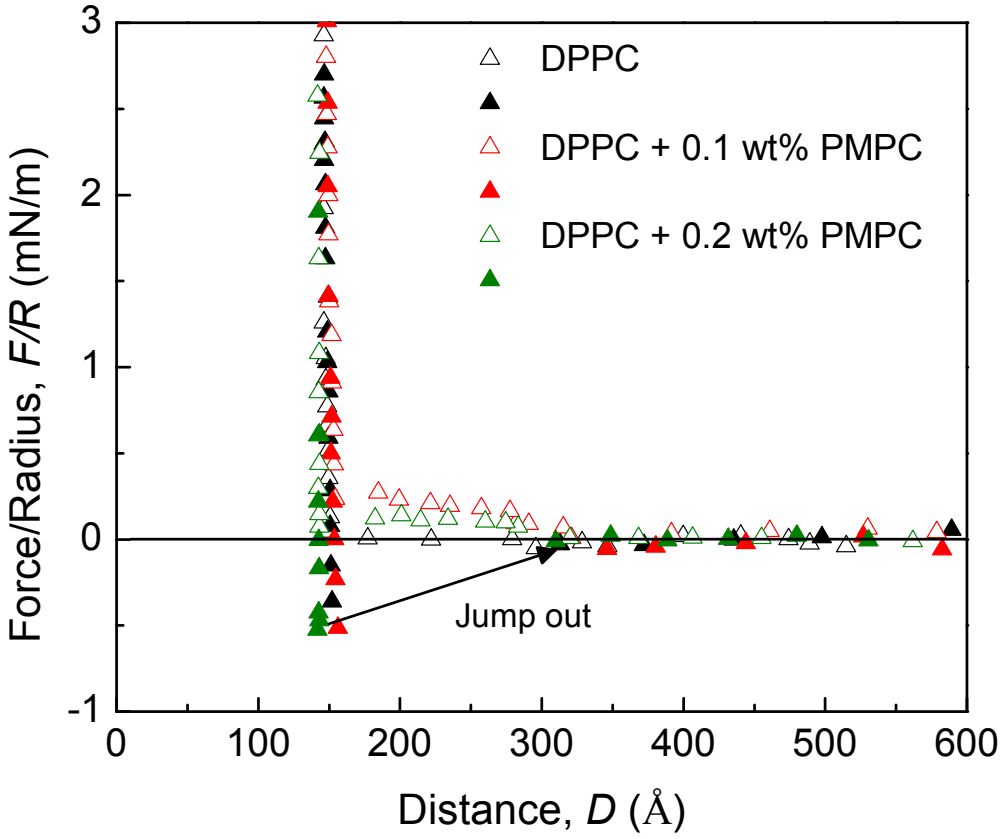

Fig. S6. Normal force−distance curves of DPPC bilayers measured at the same contact point in pure water and with the addition of 0.1 wt% and 0.2 wt% PMPC polymers. The interaction between PMPC polymer and DPPC bilayer is investigated using an SFA. Static force runs with a rate of smaller than 0.05 nm/s is performed to get equilibrium results. In pure water, pure DPPC bilayer has no surface charge and no repulsive interaction is measured during approach. Upon separation, a weak adhesion force, ~ -0.5 mN/m, is measured due to van der Waals interaction of lipid bilayers. Adding 0.1 wt% and 0.2 wt% PMPC polymers in to the solution, introduce a weak repulsion between two bilayers, indicating weak adsorption of PMPC polymer on DPPC membrane. Further compress the two bilayer surfaces gives identical force profiles as these measured

between pure DPPC bilayers, which implies that the PMPC polymers gets squeezed out of the contact area under compression, another indication of weak PMPC adsorption.

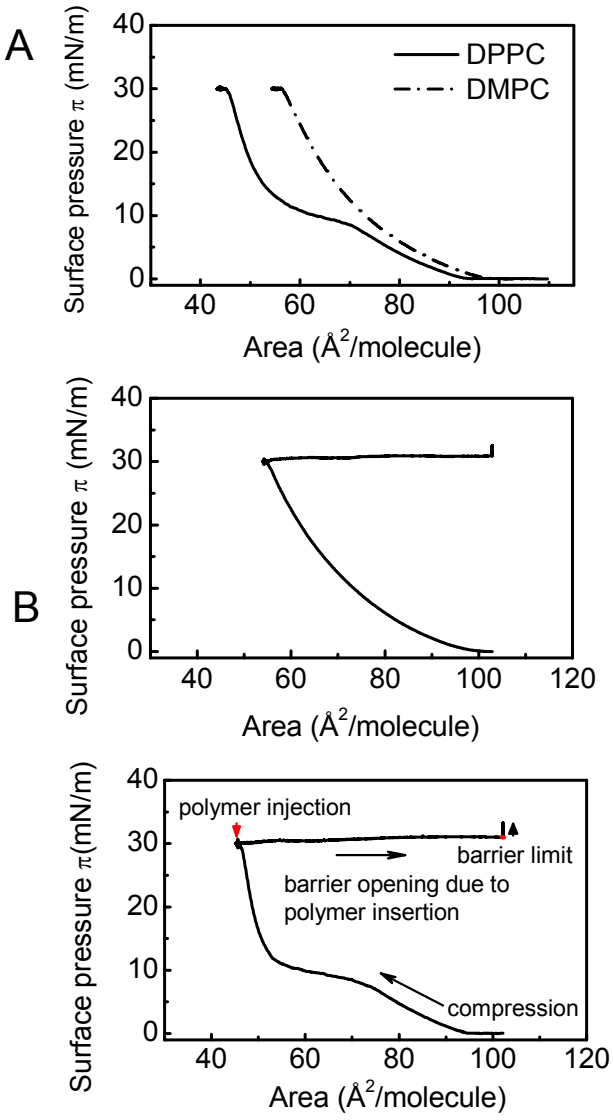

C

Fig. S7 Pressure-area isotherms of (A) DPPC and DMPC monolayers, (B) DPPC, and (C) DMPC monolayers upon insertion of BCP_6.5K[14] when the monolayers were held at the constant pressure of 30 mN/m and 25 ºC. The concentration of BCP_6.5K[14] in the water subphase is 100 μmol/L. The different stages of the experiment, such as film compression, BCP_6.5K[14] injection, barrier opening due to polymer insertion, and the increase in surface pressure after the barrier reached its physical limitation, are indicated by arrows for the DPPC case. A plateau that characterizes the first-order transition from the disordered liquid expanded (LE) phase to the ordered liquid condensed (LC) phase is seen in the DPPC isotherm at ~ 9 mN/m but not in the DMPC isotherm. Thus, at 30 mN/m, the DPPC monolayer represents a more ordered film with high lipid packing density, whereas the DMPC monolayer remains as a disordered, fluidic film. For BCP_6.5K[14], it inserts into both lipid films so greatly that the barrier of the trough was quickly expanded to its fully open position to maintain the target surface pressure. Because the copolymer continued to insert into the monolayers even after the barrier reached its physical limitation, the lipids were forced into a more densely packed layer which resulted in a further increase in surface pressure from 30 mN/m to 33 mN/m for both lipid systems.

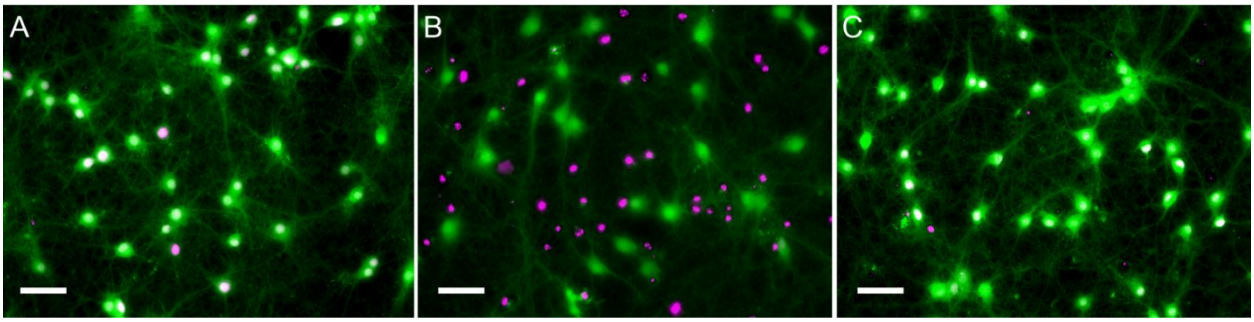

Fig. S8 Representative fluorescence images of hippocampal neurons labeled with calcein (green) and DAPI (magenta) following 45 min OGD. (A) OGD; (B) OGD followed by the addition of BCP_22K[66] for 12 h; (C) control without OGD. Scale bar: 50 μm. Note: neurons stained by both DAPI and calcein are identified as live; neurons stained only by DAPI are categorized as dead.

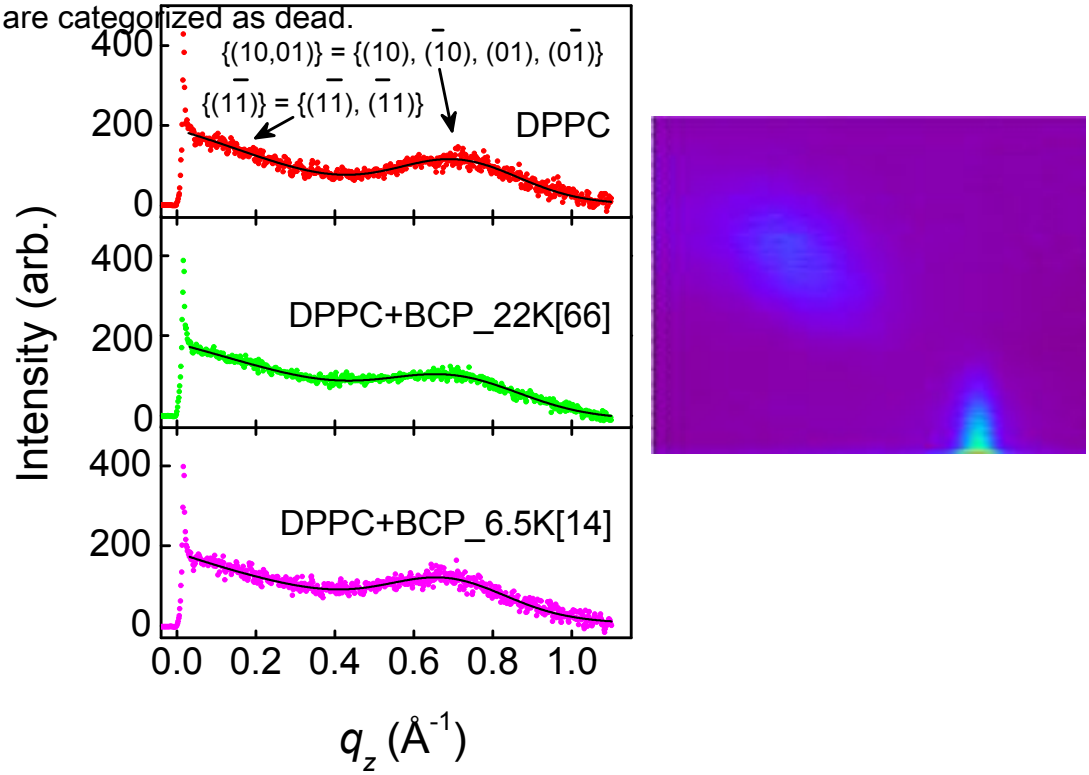

Fig. S9 Left: Bragg rods from GIXD on the pure DPPC monolayer (top panel), and DPPC monolayer in the presence of BCP_22K[66] (middle panel) and BCP_6.5K[14] (bottom panel) in the water subphase at π = 30 mN/m and T = 22 ºC. Right: 2D GIXD image. The two peaks observed in the three DPPC monolayers indicate distorted-hexagonal packing of the lipid tails in a 2-D unit cell and the corresponding Miller indices are indicated for each peak. The analysis of Bragg rods gives the molecular tilt angle relative to surface normal, θ, as 30º for DPPC and DPPC in the presence of BCP_22K[66], and 28.3º for BCP_6.5K. GIXD measurements were taken at A_{DPPC} = 47.3 Å^2, $A_{DPPC+BCP\_22K[66]}$ = 47.3 Å^2 and $A_{DPPC+BCP\_6.5K[14]}$ = 61 Å^2.

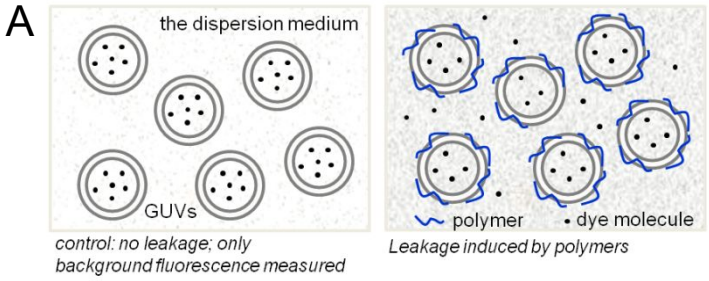

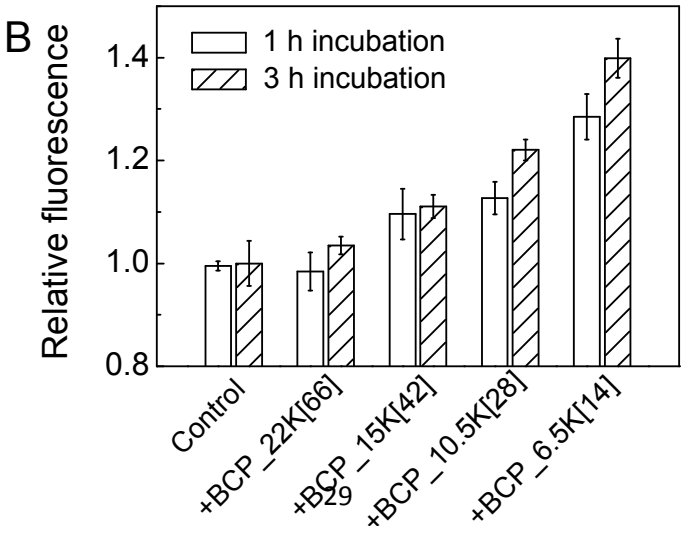

Fig. S10 (A) Scheme of the leakage assay. (B) Relative fluorescence measured from the dispersion medium of POPC GUVs, POPC GUVs in the presence of a concentration of 30 μmol/L of BCP_22K[66], BCP_15K[42], BCP_10.5K[28] and BCP_6.5K[14] for 1 and 3 h incubation period at 25 ºC. Leakage, defined by $I/I_0 > 1$, was monitored via the fluorescence increase in the dispersion medium of GUVs when Alexa 488 was leaked out from the interior of the GUVs into its external solution. Because all samples contained the same concentration of vesicles, the increase in I/I_0 with polymer hydrophobicity suggests that polymer enhanced membrane permeability also depends on its hydrophobicity. In fact, this observation is in good agreement with the insertion assay, and thus supports our argument that the insertion of these copolymers into the lipid membrane disrupts lipid packing and promotes the formation of membrane defects.

Representative characterization data for PMPC-PPO-PMPC triblock copolymers

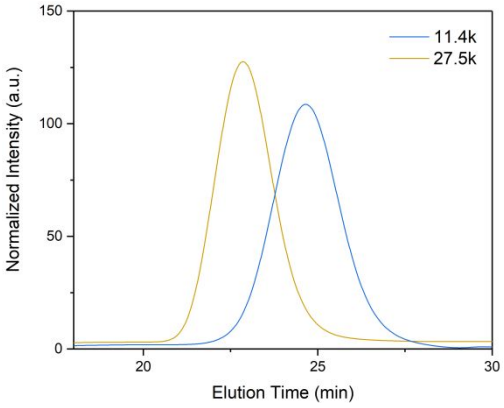

Molecular weight and polydispersity index values were estimated by gel permeation chromatography (GPC) by eluting in trifluoroethanol (TFE) which contained 0.02 M sodium trifluoroacetate. The molecular weight estimation was calibrated against narrow polydispersity poly(methyl methacrylate) (PMMA) as GPC calibration standards. The GPC analysis was performed at 40 °C with a flow rate of 1.0 mg/mL using an Agilent 1260 isocratic pump, an autosampler, a Polymer Standards Service (PSS) PFG guard column (50 mm × 8 mm), three PSS PFG linear M columns (300 mm × 8 mm, particle size 7 μm), and an Agilent 1260 refractive index detector. The data shown in the figure above is for samples with estimated molecular weights of 11.4 kDa and 27.5 kDa.

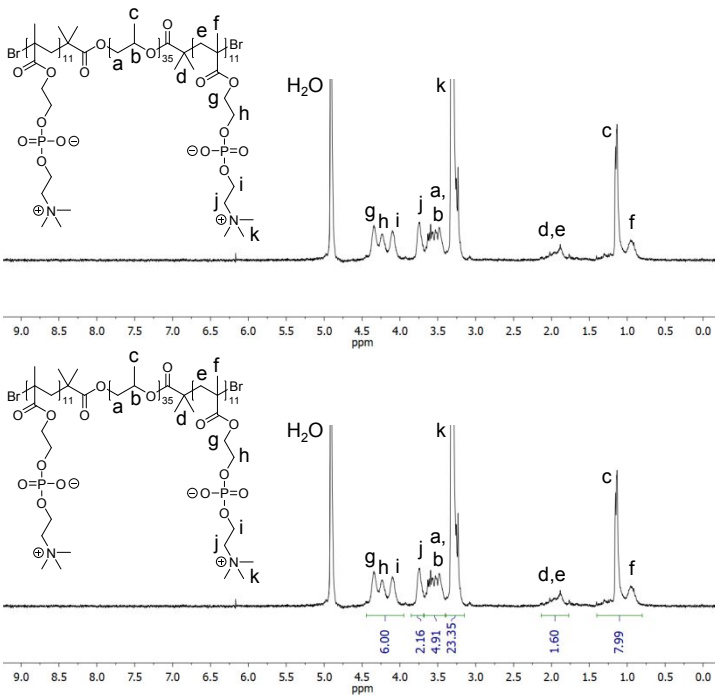

PMPC-PPO-PMPC characterization by ^{1}H NMR spectroscopy was performed using a Bruker Ascend 500 MHz spectrometer equipped with a Prodigy cryoprobe. Degree of MPC polymerization was estimated by comparing NMR signal intensities at 3.95-4.45 ppm (corresponding to MPC methylene protons *g*, *h*, and *i*) to that of PPO backbone protons *a* and *b* (3.41-3.68 ppm).

Disclaimer

Mention of any commercial products or services in this paper does not imply approval or endorsement by NIST, nor does it imply that such products or services are necessarily the best available for the purpose.

Reference:

1. X. Chen, S. McRae, S. Parelkar, T. Emrick, Polymeric phosphorylcholine-camptothecin conjugates prepared by controlled free radical polymerization and click chemistry. *Bioconjugate Chemistry* **20**, 2331 (Dec, 2009).

2. J. D. Marks, C. Boriboun, J. Wang, Mitochondrial nitric oxide mediates decreased vulnerability of hippocampal neurons from immature animals to NMDA. *The Journal of Neuroscience : the Official Journal of the Society for Neuroscience* **25**, 6561 (Jul 13, 2005).

3. L. Tung, G. C. Troiano, V. Sharma, R. M. Raphael, K. Stebe, Changes in elelctroporation thresholds of lipid membranes by surfactants and peptides. *Annals of the New York Academy of Sciences* **888**, 249-265 (1999).

4. N. Rosov, S. Rathgeber, M. Monkenbusch, Chapter 7 in Scattering from Polymers: Characterization by X-rays, Neutrons, and Light. *ACS Symp Ser* **739** 103-106 (2000) eISBN 9780841217379.

5. M. Monkenbusch, R. Schätzler, D. Richter, The Jülich neutron spin-echo spectrometer — Design and performance. *Nucl Instrum Meth A* **399**, 301 (1997).

6. R. T. Azuah *et al.*, *J Res Natl Inst Stand Technol* **114**, 341 (2009).

7. A. G. Zilmanm, R. Granek, Undulations and Dynamic Structure Factor of Membranes. *Phys Rev Lett* **77**, 4788 (1996).

8. B. H. Zimm, G. M. Roe, L. F. Epstein, Solution of a Characteristic Value Problem from the Theory of Chain Molecules. *The Journal of Chemical Physics* **24**, 279 (1956).

9. M. C. Watson, F. L. Brown, Interpreting membrane scattering experiments at the mesoscale: the contribution of dissipation within the bilayer. *Biophysical journal* **98**, L9 (Mar 17, 2010).

10. A. C. Woodka, P. D. Butler, L. Porcar, B. Farago, M. Nagao, Lipid Bilayers and Membrane Dynamics: Insight into Thickness Fluctuations. *Phys Rev Lett* **109**, (Jul 31, 2012).

11. D. Violette, P. G. DeGennes, *Physics* **3**, 181 (1967).

12. C. J. Glinka, Barker, J.G., Hammouda, B., Krueder, S., Moyer, J.J., Orts, W.J. *J Appl Crystallogr* **31**, 430-435 (1998).

13. S.M. Choi, J. G. Barker, C. J. Glinka, Y. T. Cheng, P. L. Gammel, *J Appl Crystallogr* **33**, 793-796 (2000).

14. G. W. Lynn *et al.*, Bio-SANS–a dedicated facility for neutron structural biology at Oak Ridge National Laboratory. *Physica B Condensed Matter* **880**, 385-386 (2006).

15. S. R. Kline, *J Appl Crystallogr* **39**, 895-900 (2006).

16. A. Nelson, Co-refinement of multiple-contrast neutron/X-ray reflectivity data using MOTOFIT. *J Appl Crystallogr* **39**, 273 (Apr, 2006).

17. P. A. Kienzle, K. V. O'Donovan, J. F. Ankner, N. F. Berk, C. F. Majkrzak, *http://www.ncnr.nist.gov/reflpak* (2000-2006).

18. G. Wu *et al.*, Interaction between lipid monolayers and poloxamer 188: an X-ray reflectivity and diffraction study. *Biophysical journal* **89**, 3159 (Nov, 2005).